Article

A Comparative Study of Electron Radiation Responses of Pu$_2$Zr$_2$O$_7$ and La$_2$Zr$_2$O$_7$: An *ab initio* Molecular Dynamics Study

Shounuo Zhang [1], Menglu Li [1], Haiyan Xiao [1,*], Zijiang Liu [2,*] and Xiaotao Zu [1]

[1] School of Physics, University of Electronic Science and Technology of China, Chengdu 610054, China; 201821120122@std.uestc.edu.cn (S.Z.); 202011120518@std.uestc.edu.cn (M.L.); xtzu@uestc.edu.cn (X.Z.)
[2] Department of Physics, Lanzhou City University, Lanzhou 730070, China
* Correspondence: hyxiao@uestc.edu.cn (H.X.); lzcu@lzcu.edu.cn (Z.L.)

Abstract: In this study, the response of Pu$_2$Zr$_2$O$_7$ and La$_2$Zr$_2$O$_7$ to electronic radiation is simulated, employing an *ab initio* molecular dynamics method. It is shown that Pu$_2$Zr$_2$O$_7$ undergoes a crystalline-to-amorphous structural transition with 0.3% electronic excitation, while for La$_2$Zr$_2$O$_7$, the structural amorphization occurs with 1.2% electronic excitation. During the microstructural evolution, the anion disorder further drives cation disorder and eventually results in the structural amorphization of Pu$_2$Zr$_2$O$_7$ and La$_2$Zr$_2$O$_7$. The difference in responses to electron radiation between Pu$_2$Zr$_2$O$_7$ and La$_2$Zr$_2$O$_7$ mainly results from the strong correlation effects between Pu 5f electrons and the smaller band gap of Pu$_2$Zr$_2$O$_7$. These results suggest that Pu$_2$Zr$_2$O$_7$ is less resistant to amorphization under local ionization rates that produce a low level of electronic excitation, since the level of the concentration of excited electrons is relatively low in Pu$_2$Zr$_2$O$_7$. The presented results will advance the understanding of the radiation damage effects of zirconate pyrochlores.

1. Introduction

With the growing demand for nuclear power, the problem of how to treat nuclear waste safely, especially long-lived transuranic (TRU) elements such as plutonium (Pu) and minor actinides (Np, Am) that are generated through spent fuel, has become extremely important [1–3]. Pyrochlore-structured oxides with the general formula A$_2$B$_2$O$_7$ (A = Y or another rare earth element; B = Ti, Zr, Sn, or Hf) [4] exhibit a wide range of physical, chemical, and electrical properties, including high ionic conductivity, superconductivity, luminescence, and ferromagnetism [3]. A$_2$B$_2$O$_7$ pyrochlores, thus, are taken as attractive candidates for a variety of applications, including hosts for oxidation catalysts, solid electrolytes, oxygen gas sensors, as well as ceramic thermal barrier coatings [5–7]. Particularly great efforts have been devoted to evaluating the potential of pyrochlores as host matrices for immobilization of TRU elements [4,8,9].

Zirconate pyrochlores possess high thermal stability, high chemical durability, and remarkable resistance to radiation-induced amorphization, therefore being of special interest [10–13]. Wang et al. reported that Gd$_2$(Zr$_x$Ti$_{1-x}$)$_2$O$_7$ systems (x = 0, 0.25, 0.5, 0.75, 1) become increasingly radiation resistant with increasing zirconium content under 1 MeV Kr$^+$ irradiation [14]. Lian et al. found that among a series of A$_2$Zr$_2$O$_7$ pyrochlores (A = La, Nd, Sm, and Gd), only La$_2$Zr$_2$O$_7$ can be amorphized under ion-beam irradiation [15]. Sickafus and coworkers studied the irradiation response of Er$_2$Zr$_2$O$_7$ at a dose as high as 140 dpa by 350 KeV Xe$^+$ at room temperature and found that Er$_2$Zr$_2$O$_7$ cannot be amorphized [16]. Therefore, zirconate pyrochlores would be excellent candidate host matrices for the immobilization of plutonium (Pu) and minor actinides.

In the literature [17–22], atomic collision, electronic excitation, and ionization arising from the electronic energy loss of energetic ions have been used to explain the mechanisms of irradiation-induced amorphization. Sattonnay et al. investigated how the composition affects the behavior of pyrochlores under swift heavy ions irradiation and proposed that the susceptibility to amorphization by high electronic excitation is proportional to the cation radii ratio r_A/r_B [23]. Theoretically, the influence of low electronic excitation on microstructural evolution in titanate pyrochlores was explored by Xiao et al., who, using an *ab initio* molecular dynamics (AIMD) method, predicted that structural amorphization occurs under 2% electronic excitation at room temperature [24]. Sassi et al. investigated the interplay between electronic excitation, structure, and composition in lanthanum-based ceramics employing a similar method. They found that when monoclinic-layered perovskite $La_2Ti_2O_7$ is exposed to a lower degree of electronic excitation, the amorphous transition occurs, whereas a similar phenomenon does not occur in cubic pyrochlore $La_2Zr_2O_7$ [25]. Furthermore, their results show that $La_2Zr_2O_7$ can be amorphized at 200 K under 1.6% electronic excitation. These studies demonstrate that electronic excitation may have substantial effects on the microstructural evolution and physical properties of materials.

Thus far, it is not clear how $Pu_2Zr_2O_7$ pyrochlore, which is a product for immobilization of Pu in zirconate pyrochlores [26–29], responds to electronic excitation. In this study, a comparative study of the responses of $Pu_2Zr_2O_7$ and $La_2Zr_2O_7$ to electronic excitation is made to explore the behaviors of $Pu_2Zr_2O_7$ under electronic radiation. It is noted that discrepancies exist in microstructural evolution under electronic excitation between $Pu_2Zr_2O_7$ and $La_2Zr_2O_7$. The possible reasons have also been explored. The presented results thus gain fundamental insights into the radiation damage effects of $Pu_2Zr_2O_7$ and may promote related experimental investigations.

2. Computational Details

Our calculations are carried out by the *ab initio* molecular dynamics (AIMD) method, as implemented in the Vienna Ab Initio Simulation Package (It was developed by the University of Vienna) (VASP) code [30,31]. In order to describe the exchange-correlation effects between electrons, the generalized gradient approximation (GGA) as parametrized by Perdew and Wang is used [32]. Because AIMD simulation is computationally very expensive, a $1 \times 1 \times 1$ Monkhorst-Pack grid was generally employed in the AIMD simulation [24,33,34]. Hence, a $1 \times 1 \times 1$ Monkhorst-Pack grid is employed in this study as a compromise between computational efficiency and computational accuracy. Computations are performed with a cutoff energy of 300 eV for the plane wave basis set. In our calculations, we employ a $2 \times 2 \times 2$ supercell containing 88 atoms. The Hubbard U correction [35] is considered to modify the strongly correlated Pu 5*f* electrons, and a U_{eff} value of 4 eV is employed [36].

To study the effect of electronic excitation, we remove several electrons from high-lying valence band states. A jellium background is used to compensate for the loss of charge due to electron removal. Within this approximation, one assumes that electrons move in the presence of a neutralizing background consisting of uniformly spread positive charge [37]. After the system reaches equilibrium states, the removed electrons are placed back to mimic the recombination of electrons and holes. This method has made it possible to simulate the role of electronic excitation and has been applied to simulate the structural amorphization of Ge–Sb–Te alloys [38] and pyrochlores [24,25]. For $La_2Zr_2O_7$ and $Pu_2Zr_2O_7$, the considered electronic excitation concentrations are 0.3%, 0.6%, and 1.2%. Here, the percentage of electronic excitation concentration corresponds to the number of excited valence electrons to the number of total electrons. The intensity of the e–h pairs that are generated can be estimated by $N_{e\text{-}h} = \frac{(1-R) \times \alpha_{eff} \times F}{\hbar \omega_0}$ [39], where F and ω_0 are the laser fluence and frequency, and R and α_{eff} are the reflectivity and effective absorption coefficient for the sample [40–43]. Under laser beam irradiation, the laser fluence at 400 nm for 1% excitation in $La_2Zr_2O_7$ is about 8.6×10^2–4.9×10^3 mJ/cm^2. The AIMD simulation is conducted

employing an isothermal–isochoric ensemble, and the temperature is controlled by the Nosé–Hoover thermostat. The simulation time is 6 ps, and the time step is 3 fs.

3. Results and Discussions

3.1. Ground State Properties of $Pu_2Zr_2O_7$ and $La_2Zr_2O_7$

Structural optimization is first performed on $Pu_2Zr_2O_7$ and $La_2Zr_2O_7$. The Schematic view of the geometrical structures of $La_2Zr_2O_7$ is shown in Figure 1. The calculated lattice constants, oxygen positional parameter x_{O8f}, as well as bonding distances for $Pu_2Zr_2O_7$ and $La_2Zr_2O_7$, are summarized in Table 1, along with the available theoretical and experimental results for comparison. For $Pu_2Zr_2O_7$, the obtained lattice constant of 10.802 Å is slightly larger than the experimental value of 10.70 Å [44], whereas it is consistent with the theoretical result of 10.802 Å [36]. The lattice constant of $La_2Zr_2O_7$ is determined to be 10.879 Å, which is in reasonable agreement with the experimental value of 10.805 Å [45] and comparable to the calculated value of 10.696 Å [2]. The relatively larger lattice constant for La2Zr2O7 is mainly due to its larger ionic radius, i.e., ~1.16 Å for La^{3+} and ~1.1 Å for Pu^{3+} [46]. With regard to oxygen positional parameter x_{O48f}, the calculated value of 0.335 for $Pu_2Zr_2O_7$ is the same as other calculations of 0.335 [36]. For $La_2Zr_2O_7$, the calculated value of 0.333 agrees well with the experimental and other calculated values [2,45]. Generally, the pyrochlores with the x_{O48f} value being closer to 0.375 are more resistant to structural amorphization under ion irradiation [26,47]. It is noted that the x_{O48f} value for $Pu_2Zr_2O_7$ is slightly larger than that of $La_2Zr_2O_7$, suggesting that $Pu_2Zr_2O_7$ and $La_2Zr_2O_7$ may have different responses to ion irradiation.

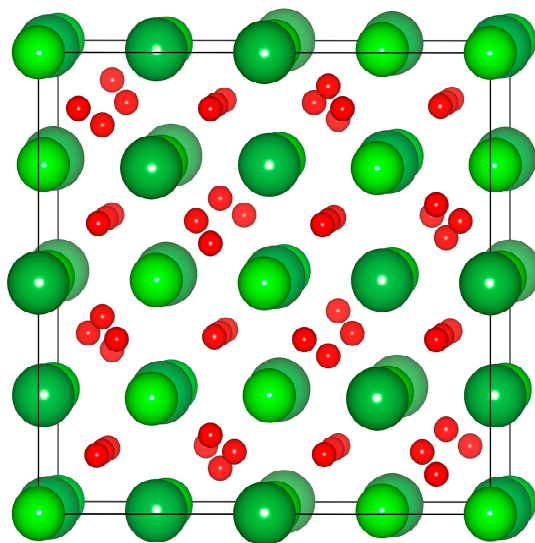**Figure 1.** Schematic view of the geometrical structures of $La_2Zr_2O_7$. The dark green, yellow-green, and red spheres represent La, Zr, and O atoms, respectively.

Table 1. The calculated lattice constants a_0 (Å), O_{48f} position parameter x (x_{O48f}), and bonding distances (Å) for $La_2Zr_2O_7$ and $Pu_2Zr_2O_7$. E_g represents the band gap; d<A-B>: bonding distances between A and B atoms (A = La, Pu, or Zr; B = O_{48f} or O_{8b}).

Compounds	a_0	x_{O48f}	Eg (eV)	d<La-O$_{48f}$>	d<La-O$_{8b}$>	d<Pu-O$_{48f}$>	d<Pu-O$_{8b}$>	d<Zr-O$_{48f}$>
$La_2Zr_2O_7$	10.879	0.333	3.58	2.635	2.339	–	–	2.106
Cal. [2]	10.696	0.3346	3.52	2.589	2.316	–	–	2.096
Exp. [45]	10.805	0.332	–	2.635	2.339	–	–	2.105
$Pu_2Zr_2O_7$	10.802	0.335	2.12	–	–	2.587	2.317	2.099
Cal. [36]	10.802	0.335	2.37	–	–	2.615	2.339	2.117
Exp. [44]	10.70	–	–	–	–	–	–	–

3.2. Microstructural Evolution in La$_2$Zr$_2$O$_7$ under Electronic Excitation

In order to explore the response of La$_2$Zr$_2$O$_7$ to electronic radiation, AIMD simulations are first carried out with an electronic excitation concentration of 0.3%. Figure 2 shows a variation of temperature and total energy with time for La$_2$Zr$_2$O$_7$ with 0.3% electronic excitation at 300 K. It is obvious that the simulation time of 6 ps is long enough so that the system can reach equilibrium states.
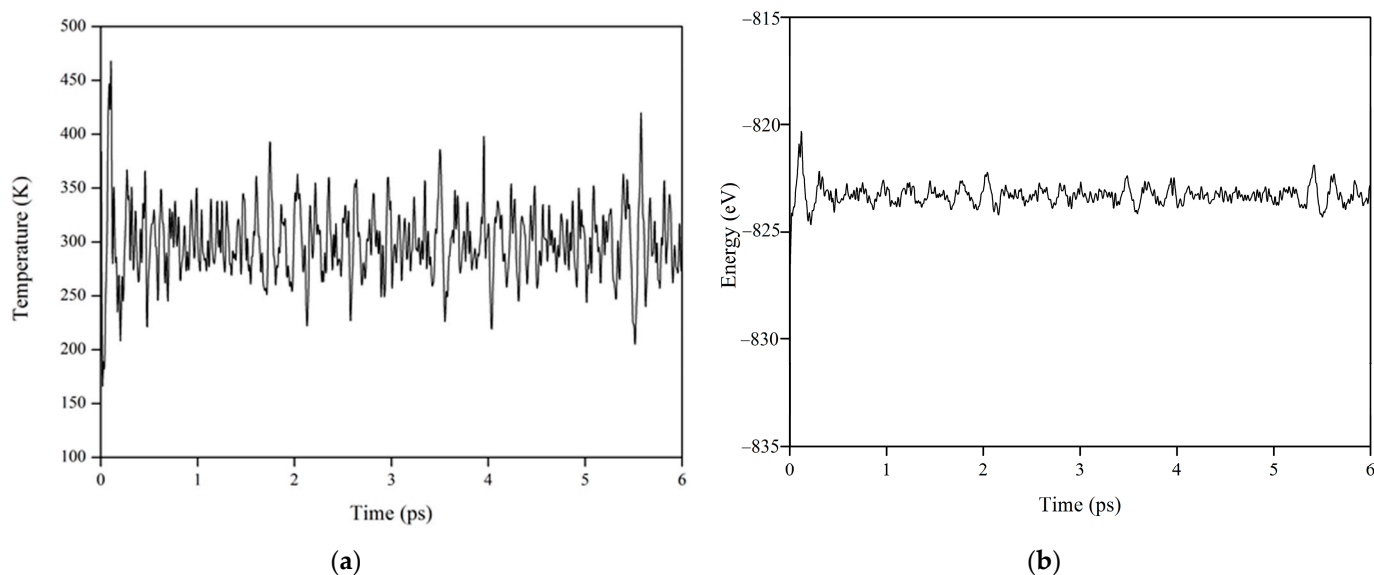

(**a**)　　　　　　　　　　　　　　　　　　　　　　　　　　　　(**b**)

Figure 2. Variation of (**a**) temperature and (**b**) total energy with time for La$_2$Zr$_2$O$_7$ with 0.3% electron excitation.

To investigate how the electronic excitation concentration affects microstructural evolution in La$_2$Zr$_2$O$_7$ at 300 K, electronic excitation concentration of 0.3%, 0.6%, 1.2%, and 1.6% are considered. Based on each equilibrium state, the radial distribution function (RDF) analysis is then carried out. Figure 3 shows the RDF for La$_2$Zr$_2$O$_7$ with 0.3%, 0.6%, 1.2%, and 1.6% electronic excitations. For electronic excitations of 0.3%, 0.6%, and 1.2%, it is noted that the structure is ordered at both short-range and long-range distances, meaning that La$_2$Zr$_2$O$_7$ still remains a pyrochlore structure. Here, the short-range correlation means the bonding interaction, and the long-range correlation corresponds to a nonbonding interaction. In the case of 1.6% electronic excitation, the structure retains a short-range order but has lost its long-range order, suggesting that 1.6% electronic excitation can induce a crystalline-to-amorphous transition in La$_2$Zr$_2$O$_7$ at room temperature. In the literature, a similar phenomenon was observed by Sassi et al. [25]. Variation of RDF with time for La$_2$Zr$_2$O$_7$ with 1.6% electronic excitation is displayed in Figure 4a. It is shown that the structural amorphization starts at t = 0.075 ps and the structure is completely amorphized at t = 0.3 ps, i.e., under 1.6% electronic excitation the crystalline-to-amorphous transition occurs very fast.

Figure 4b shows a schematic view of the geometrical structure for La$_2$Zr$_2$O$_7$ with 1.6% electronic excitation. Compared with the pyrochlore structure presented in Figure 1, it can be seen that the structure is disordered after 1.6% electronic excitation. Furthermore, the degree of anion disorder is much larger than that of cation disorder. We also explore the variation of mean square displacement (MSD) with time for La$_2$Zr$_2$O$_7$ with 1.6% electronic excitation, and the results are presented in Figure 4c. It is found that the mean square displacement of oxygen is considerably larger than that of La and Zr. These results indicate that the displacement of oxygen drives the pyrochlore of La$_2$Zr$_2$O$_7$ to undergo a crystalline-to-amorphous transition under 1.6% electronic excitation. Theoretically, Xiao et al. also suggested that the amorphization of titanate pyrochlores is mainly contributed by the displacement of oxygens [24]. Experimentally, Lian et al. found that under ion irradiation,

anion disorder precedes cation disorder in $Gd_2Ti_2O_7$, $Er_2Ti_2O_7$, and $La_2Ti_2O_7$ [48]. In this study, it is noted that the MSD increases with the increasing time rather than vibrates slightly after the system reaches equilibrium states. A similar phenomenon has been found in the literature [49], where the La/Zr/O atoms in the amorphous structure also diffuse rather than vibrate at their equilibrium sites.
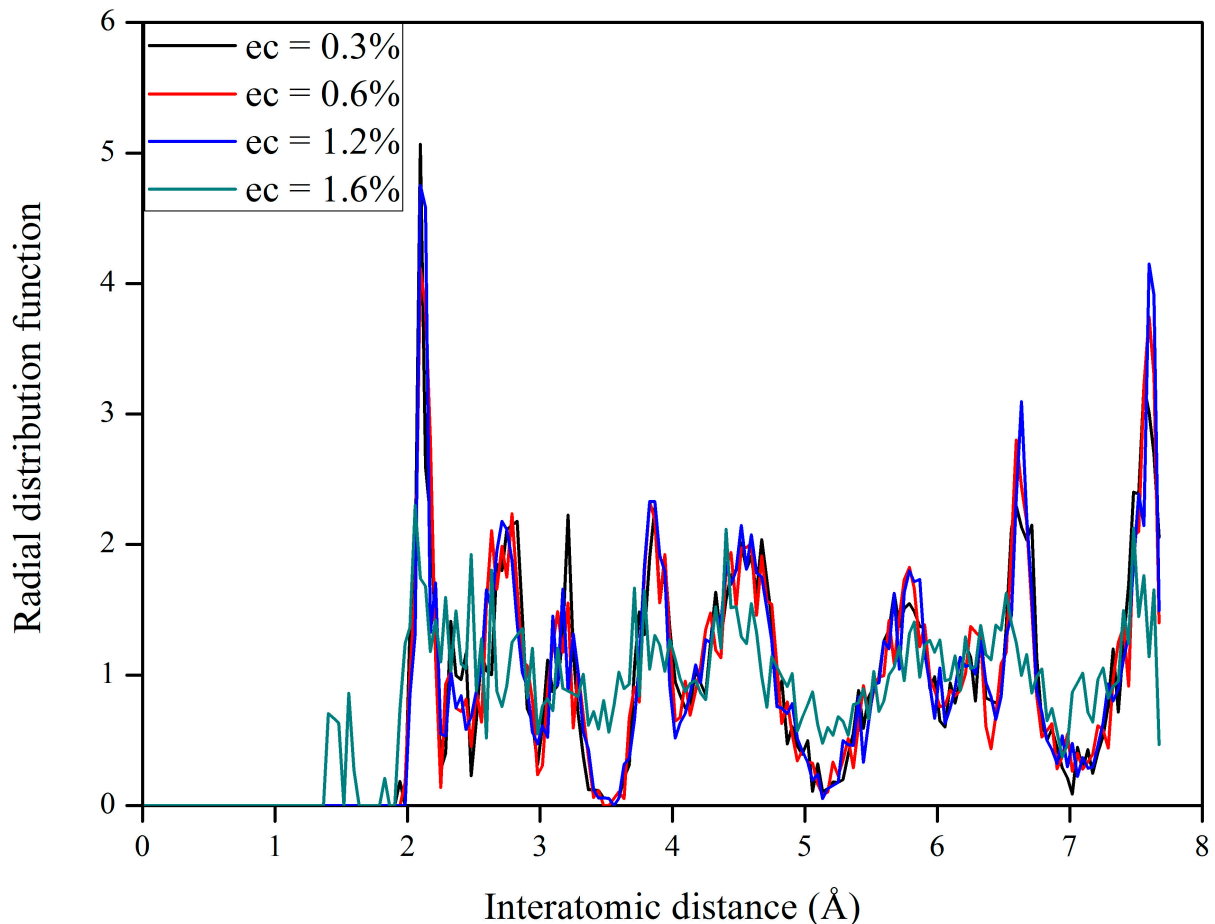

Figure 3. Radial distribution function (RDF) for $La_2Zr_2O_7$ with 0.3%, 0.6%, 1.2%, and 1.6% electron excitations.

3.3. Microstructural Evolution in $Pu_2Zr_2O_7$ under Electronic Excitation

To explore how the $Pu_2Zr_2O_7$ pyrochlore responds to electronic excitation, AIMD simulation is also carried out on $Pu_2Zr_2O_7$, in which 0.3% electrons are excited at 300 K. The corresponding variation of RDF with time for $Pu_2Zr_2O_7$ with 0.3% electronic excitation is illustrated in Figure 5a. We found that at t = 0.3 ps the structure becomes disordered at a long-range distance, and with time evolution, the structure is eventually completely amorphized. Compared with the case of $La_2Zr_2O_7$, the crystalline-to-amorphous transition occurs more easily in $Pu_2Zr_2O_7$, since the threshold electronic concentration of 0.3% is much lower than that of 1.6% for $La_2Zr_2O_7$. These results suggest that the $Pu_2Zr_2O_7$ should be readily amorphized under local ionization rates that produce a low level of electronic excitation. Theoretically, Shen et al. suggested that the influences of different types of point defects on the thermomechanical properties of $Pu_2Zr_2O_7$ and $Gd_2Zr_2O_7$ show somewhat different character, and $Pu_2Zr_2O_7$ has been suggested to be more susceptible to radiation-induced amorphization than other zirconate pyrochlores like $Gd_2Zr_2O_7$ [50].
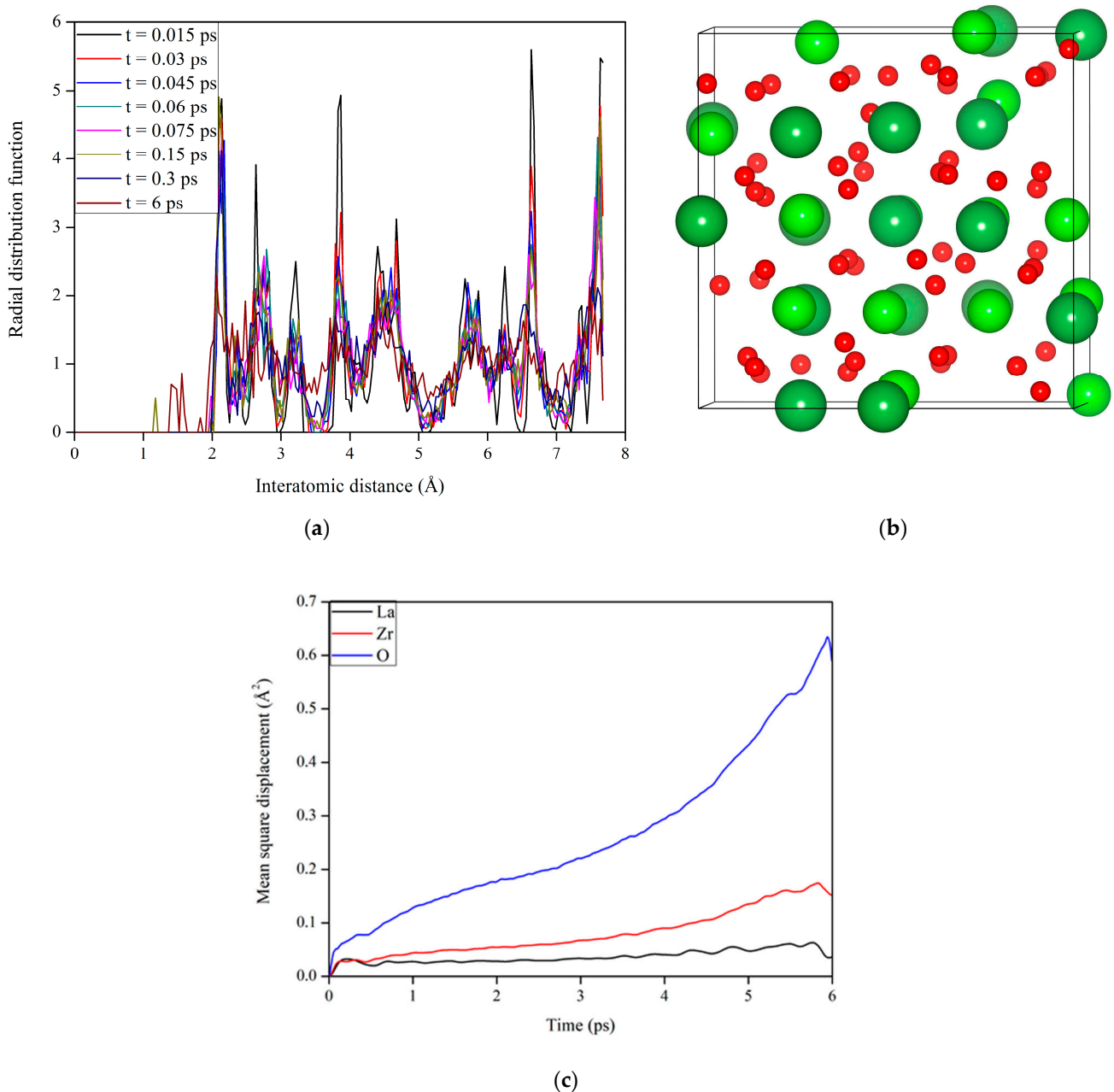
(a)

(b)

(c)

Figure 4. (**a**) Variation of radial distribution function (RDF) with time, (**b**) schematic view of the geometrical structure, and (**c**) variation of mean square displacement (MSD) with time for $La_2Zr_2O_7$ with 1.6% electron excitation.

To explore the origin of the structural amorphization induced by electronic excitation in $Pu_2Zr_2O_7$, we plot the variation of mean square displacement with time for $Pu_2Zr_2O_7$ with 0.3% electron excitation in Figure 5c. It is shown that the mean square displacement of anions is considerably larger than that of cations. Figure 5b also shows that the disorder of anions is more significant than that of cations. These results suggest that the structural amorphization is also driven by anion disordering, similar to the case of $La_2Zr_2O_7$ discussed above and the cases of titanate pyrochlores reported by Xiao et al. [24].

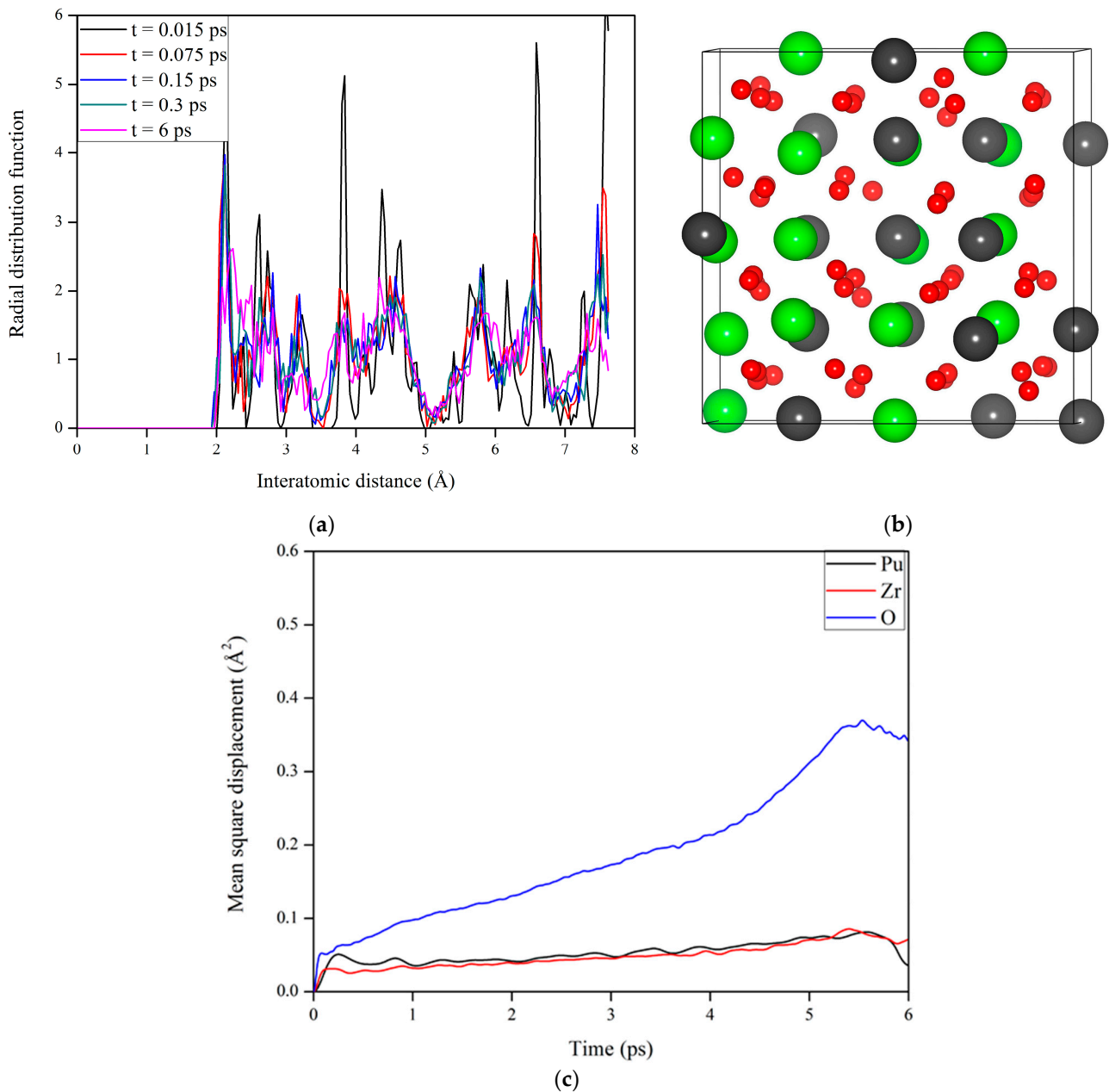**Figure 5.** (**a**) Variation of radial distribution function (RDF) with time, (**b**) schematic view of the geometrical structure, and (**c**) variation of mean square displacement (MSD) with time for $Pu_2Zr_2O_7$ with 0.3% electron excitation.

3.4. Origin of the Different Electronic Radiation Responses between $La_2Zr_2O_7$ and $Pu_2Zr_2O_7$

In order to explain the different electronic radiation responses between $Pu_2Zr_2O_7$ and $La_2Zr_2O_7$, we further analyze their geometrical and electronic structures. Comparing the bonding distances in $Pu_2Zr_2O_7$ and $La_2Zr_2O_7$ (see Table 1), we find that the values of ~2.587 Å for <Pu-O$_{48f}$>, ~2.317 Å for <Pu-O$_{8b}$>m and ~2.099 Å for <Zr-O$_{48f}$> are slightly smaller than the values of ~2.635 Å for <La-O$_{48f}$>, ~2.339 Å for <La-O$_{8b}$>, and 2.106 Å for <Zr-O$_{48f}$>, respectively. These results mean that stronger bonding interactions exist in $Pu_2Zr_2O_7$ than in $La_2Zr_2O_7$. However, the band gap of 2.12 eV for $Pu_2Zr_2O_7$ is smaller than the value of 3.52 eV for $La_2Zr_2O_7$, i.e., the valence electrons in $Pu_2Zr_2O_7$ are more easily to be excited to the conduction bands if enough energy is provided.

Figure 6 presents the total and projected density of state (DOS) distributions for ideal$La_2Zr_2O_7$ and $Pu_2Zr_2O_7$. For $La_2Zr_2O_7$ (see Figure 6a), O 2*p* orbital dominates and hybridizes with very few La 5*d* and Zr 4*d* orbitals at the valence band maximum (VBM),

and few Zr 4*d* and O 2*p* orbitals contribute to the conduction band minimum (CBM). For Pu$_2$Zr$_2$O$_7$ (see Figure 6b), it is shown that the Pu 5*f* orbital dominates and hybridizes with very few O 2*p* and Zr 4*d* orbitals at the VBM, and the CBM are contributed by Pu 5*f* orbital and very few Zr 4*d* and O 2*p* orbitals. On the one hand, because of the strong correlation effects between Pu 5*f* electrons, the O 2*p* electrons in Pu$_2$Zr$_2$O$_7$ are more readily to be excited than Pu 5*f* electrons. On the other hand, in spite of the stronger <Pu-O> bonding interaction in Pu$_2$Zr$_2$O$_7$ than the <Zr-O> bonding interaction in La$_2$Zr$_2$O$_7$ at valence bands, the O 2*p* electrons in Pu$_2$Zr$_2$O$_7$ are more easily to be excited to the conduction bands due to the much smaller band gap. Consequently, anion disorder drives cation disorder and eventually results in structural amorphization.
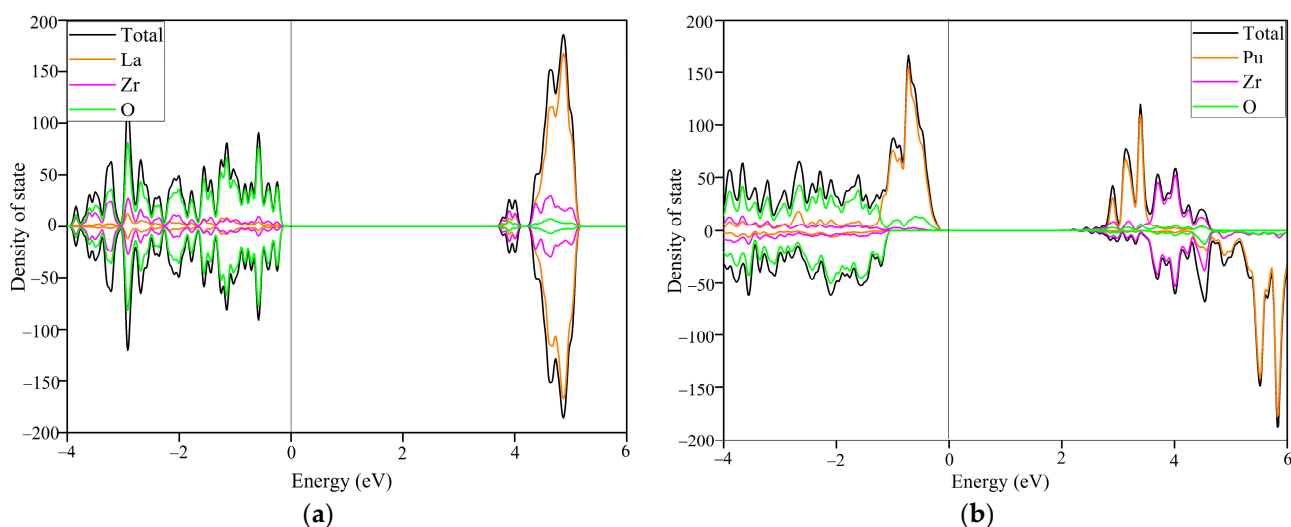

Figure 6. A comparison of the atomic projected density of state (DOS) distribution for ideal (**a**) La$_2$Zr$_2$O$_7$ and (**b**) Pu$_2$Zr$_2$O$_7$.

4. Conclusions

In summary, the microstructural evolution in Pu$_2$Zr$_2$O$_7$ and La$_2$Zr$_2$O$_7$ under electron radiation has been investigated by *ab initio* molecular dynamics simulations. It is shown that Pu$_2$Zr$_2$O$_7$ is more susceptible to electron radiation than La$_2$Zr$_2$O$_7$, since the crystalline-to-amorphous structural transition at 300 K occurs at 0.3% electronic excitation for Pu$_2$Zr$_2$O$_7$ and 1.6% for La$_2$Zr$_2$O$_7$. In both compounds, the degree of anion disorder is much larger than the degree of cation, i.e., the structural amorphization is driven by anion disorder. In Pu$_2$Zr$_2$O$_7$, there are strong correlation effects between Pu 5*f* electrons, resulting in O 2*p* electrons being more readily excited. Furthermore, the band gap of Pu$_2$Zr$_2$O$_7$ is much smaller than that of La$_2$Zr$_2$O$_7$. Consequently, the O 2*p* electrons in Pu$_2$Zr$_2$O$_7$ are more easily to be excited to the conduction bands, and Pu$_2$Zr$_2$O$_7$ is less resistant to electron radiation than La$_2$Zr$_2$O$_7$.

Author Contributions: Investigation, S.Z.; methodology, S.Z.; writing—original draft, S.Z.; writing—review & editing, M.L., H.X., Z.L. and X.Z.; formal analysis, M.L. and X.Z.; validation, M.L.; conceptualization, H.X.; supervision, H.X.; funding acquisition, Z.L.; resources, Z.L.; project administration, X.Z. All authors have read and agreed to the published version of the manuscript.

Institutional Review Board Statement: Not applicable.

Informed Consent Statement: Not applicable.

Data Availability Statement: The raw/processed data required to reproduce these findings cannot be shared at this time as the data also form part of an ongoing study.

Conflicts of Interest: The authors declare no conflict of interest.

References

1. Ewing, R.C. Nuclear waste forms for actinides. *Proc. Natl. Acad. Sci. USA* **1999**, *96*, 3432. [CrossRef] [PubMed]
2. Xiao, H.Y.; Jiang, M.; Zhao, F.A.; Liu, Z.J.; Zu, X.T. Thermal and mechanical stability, electronic structure and energetic properties of Pu-containing pyrochlores: La2−yPuyZr2O7 and La2Zr2−yPuyO7 (0 <= y <= 2) . *J. Nucl. Mater.* **2015**, *466*, 162–171. [CrossRef]
3. Ewing, R.C.; Weber, W.J.; Lian, J. Nuclear waste disposal—Pyrochlore ($A_2B_2O_7$): Nuclear waste form for the immobilization of plutonium and "minor" actinides. *J. Appl. Phys.* **2004**, *95*, 5949–5971. [CrossRef]
4. Xiao, H.Y.; Gao, F.; Weber, W.J. Ab initio investigation of phase stability of $Y_2Ti_2O_7$ and $Y_2Zr_2O_7$ under high pressure. *Phys. Rev. B* **2009**, *80*, 4. [CrossRef]
5. Moon, P.K.; Tuller, H.L. Evaluation of the $Gd_2(Zr_xTi_{1-x})_2O_7$ pyrochlore system as an oxygen gas sensor. *Sens. Actuators B: Chem.* **1990**, *1*, 199–202. [CrossRef]
6. Zhang, Z.L.; Xiao, H.Y.; Zu, X.T.; Gao, F.; Weber, W.J. First-principles calculation of structural and energetic properties for $A_2Ti_2O_7$ (A = Lu, Er, Y, Gd, Sm, Nd, La). *J. Mater. Res.* **2009**, *24*, 1335–1341. [CrossRef]
7. Xiao, H.Y.; Zu, X.T.; Gao, F.; Weber, W.J. First-principles study of energetic and electronic properties of $A_2Ti_2O_7$ (A=Sm, Gd, Er) pyrochlore. *J. Appl. Phys.* **2008**, *104*, 073503. [CrossRef]
8. Weber, W.J.; Ewing, R.C. Plutonium immobilization and radiation effects. *Science* **2000**, *289*, 2051–2052. [CrossRef]
9. Weber, W.J.; Wald, J.W.; Matzke, H. Self-radiation damage in $Gd_2Ti_2O_7$. *Mater. Lett.* **1985**, *3*, 173–180. [CrossRef]
10. Hayakawa, I.; Kamizono, H. Durability of an $La_2Zr_2O_7$ waste form in water. *J. Mater. Sci.* **1993**, *28*, 513–517. [CrossRef]
11. Kamizono, H.; Hayakawa, I.; Muraoka, S. Durability of Zirconium-Containing Ceramic Waste Forms in Water. *J. Am. Ceram. Soc.* **1991**, *74*, 863–864. [CrossRef]
12. Hayakawa, I.; Kamizono, H. Durability of an $La_2Zr_2O_7$ waste form containing various amounts of simulated HLW elements. *J. Nucl. Mater.* **1993**, *202*, 163–168. [CrossRef]
13. Sickafus, K.E.; Minervini, L.; Grimes, R.W.; Valdez, J.A.; Ishimaru, M.; Li, F.; McClellan, K.J.; Hartmann, T. Radiation tolerance of complex oxides. *Science* **2000**, *289*, 748–751. [CrossRef]
14. Wang, S.X.; Begg, B.D.; Wang, L.M.; Ewing, R.C.; Weber, W.J.; Kutty, K.V.G. Radiation stability of gadolinium zirconate: A waste form for plutonium disposition. *J. Mater. Res.* **1999**, *14*, 4470–4473. [CrossRef]
15. Lian, J.; Zu, X.T.; Kutty, K.V.G.; Chen, J.; Wang, L.M.; Ewing, R.C. Ion-irradiation-induced amorphization of $La_2Zr_2O_7$ pyrochlore. *Phys. Rev. B* **2002**, *66*, 5. [CrossRef]
16. Sickafus, K.E.; Minervini, L.; Grimes, R.W.; Valdez, J.A.; Hartmann, T. A comparison between radiation damage accumulation in oxides with pyrochlore and florite structures. *Radiat. Eff. Defects Solids* **2001**, *155*, 133–137. [CrossRef]
17. Mafi, E.; Soudi, A.; Gu, Y. Electronically Driven Amorphization in Phase-Change In2Se3 Nanowires. *J. Phys. Chem. C* **2012**, *116*, 22539–22544. [CrossRef]
18. Kolobov, A.V.; Krbal, M.; Fons, P.; Tominaga, J.; Uruga, T. Distortion-triggered loss of long-range order in solids with bonding energy hierarchy. *Nat. Chem.* **2011**, *3*, 311–316. [CrossRef] [PubMed]
19. Weber, W.J. Models and mechanisms of irradiation-induced amorphization in ceramics. *Nucl. Instrum. Methods Phys. Res. Sect. B-Beam Interact. Mater. At.* **2000**, *166*, 98–106. [CrossRef]
20. Zhang, Y.; Weber, W.J.; Shutthanandan, V.; Devanathan, R.; Thevuthasan, S.; Balakrishnan, G.; Paul, D.M. Damage evolution on Sm and O sublattices in Au-implanted samarium titanate pyrochlore. *J. Appl. Phys.* **2004**, *95*, 2866–2872. [CrossRef]
21. Jiang, C.; Stanek, C.R.; Sickafus, K.E.; Uberuaga, B.P. First-principles prediction of disordering tendencies in pyrochlore oxides. *Phys. Rev. B* **2009**, *79*, 5. [CrossRef]
22. Zhang, Y.; Bae, I.-T.; Weber, W.J. Atomic collision and ionization effects in oxides. *Nucl. Instrum. Methods Phys. Res. Sect. B Beam Interact. Mater. At.* **2008**, *266*, 2828–2833. [CrossRef]
23. Sattonnay, G.; Moll, S.; Thomé, L.; Legros, C.; Calvo, A.; Herbst-Ghysel, M.; Decorse, C.; Monnet, I. Effect of composition on the behavior of pyrochlores irradiated with swift heavy ions. *Nucl. Instrum. Methods Phys. Res. Sect. B Beam Interact. Mater. At.* **2012**, *272*, 261–265. [CrossRef]
24. Xiao, H.Y.; Weber, W.J.; Zhang, Y.; Zu, X.T.; Li, S. Electronic excitation induced amorphization in titanate pyrochlores: An ab initio molecular dynamics study. *Sci. Rep.* **2015**, *5*, 8. [CrossRef]
25. Sassi, M.; Kaspar, T.; Rosso, K.M.; Spurgeon, S.R. Effect of structure and composition on the electronic excitation induced amorphization of La2Ti2-xZrxO7 ceramics. *Sci. Rep.* **2019**, *9*, 10. [CrossRef] [PubMed]
26. Zhao, F.A.; Xiao, H.Y.; Jiang, M.; Liu, Z.J.; Zu, X.T. A DFT plus U study of Pu immobilization in Gd2Zr2O7. *J. Nucl. Mater.* **2015**, *467*, 937–948. [CrossRef]
27. Williford, R.E.; Weber, W.J. Computer simulation of Pu3+ and Pu4+ substitutions in gadolinium zirconate. *J. Nucl. Mater.* **2001**, *299*, 140–147. [CrossRef]

28. Cleave, A.; Grimes, R.W.; Sickafus, K. Plutonium and uranium accommodation in pyrochlore oxides. *Philos. Mag.* **2005**, *85*, 967–980. [CrossRef]

29. Kulkarni, N.K.; Sampath, S.; Venugopal, V. Preparation and characterisation of Pu-pyrochlore: $[La_{1-x}Pu_x]_2 Zr_2O_7$ (x=0–1). *J. Nucl. Mater.* **2000**, *281*, 248–250. [CrossRef]

30. Kresse, G.; Furthmuller, J. Efficient iterative schemes for ab initio total-energy calculations using a plane-wave basis set. *Phys. Rev. B* **1996**, *54*, 11169–11186. [CrossRef]

31. Kresse, G.; Furthmuller, J. Efficiency of ab-initio total energy calculations for metals and semiconductors using a plane-wave basis set. *Comput. Mater. Sci.* **1996**, *6*, 15–50. [CrossRef]

32. Wang, Y.; Perdew, J.P. Correlation hole of the spin-polarized electron-gas, with exact small-wave-vector and high-density scaling. *Phys. Rev. B* **1991**, *44*, 13298–13307. [CrossRef] [PubMed]

33. Jiang, M.; Gong, H.; Zhou, B.; Xiao, H.; Zhang, H.; Liu, Z.; Zu, X. An AIMD+U simulation of low-energy displacement events in UO2. *J. Nucl. Mater.* **2020**, *540*, 152379. [CrossRef]

34. Jiang, M.; Xiao, H.; Peng, S.; Yang, G.; Gong, H.; Liu, Z.; Qiao, L.; Zu, X. Ab initio molecular dynamics simulation of the radiation damage effects of GaAs/AlGaAs superlattice. *J. Nucl. Mater.* **2019**, *516*, 228–237. [CrossRef]

35. Dudarev, S.L.; Botton, G.A.; Savrasov, S.Y.; Humphreys, C.J.; Sutton, A.P. Electron-energy-loss spectra and the structural stability of nickel oxide: An LSDA+U study. *Phys. Rev. B* **1998**, *57*, 1505–1509. [CrossRef]

36. Li, P.C.; Zhao, F.G.; Xiao, H.Y.; Zhang, H.B.; Gong, H.F.; Zhang, S.; Liu, Z.J.; Zu, X.T. First-Principles Study of Thermo-Physical Properties of Pu-Containing $Gd_2Zr_2O_7$. *Nanomaterials* **2019**, *9*, 196. [CrossRef] [PubMed]

37. Ciftja, O.; Escamilla, L.; Mills, R. Shape-Dependent Energy of an Elliptical Jellium Background. *Adv. Condens. Matter Phys.* **2015**, *2015*, 851356. [CrossRef]

38. Li, X.B.; Liu, X.Q.; Liu, X.; Han, D.; Zhang, Z.; Han, X.D.; Sun, H.B.; Zhang, S.B. Role of Electronic Excitation in the Amorphization of Ge-Sb-Te Alloys. *Phys. Rev. Lett.* **2011**, *107*, 4. [CrossRef] [PubMed]

39. Sokolowskitinten, K.; Bialkowski, J.; Vonderlinde, D. Ultrafast laser-induced order-disorder transitions in semiconductors. *Phys. Rev. B* **1995**, *51*, 14186–14198. [CrossRef] [PubMed]

40. Weller, M.T.; Hughes, R.W.; Rooke, J.; Knee, C.S.; Reading, J. The pyrochlore family—A potential panacea for the frustrated perovskite chemist. *Dalton Trans.* **2004**, 3032–3041. [CrossRef]

41. Malkin, B.Z.; Zakirov, A.R.; Popova, M.N.; Klimin, S.A.; Chukalina, E.P.; Antic-Fidancev, E.; Goldner, P.; Aschehoug, P.; Dhalenne, G. Optical spectroscopy of $Yb_2Ti_2O_7$ and $Y_2Ti_2O_7$: Yb^{3+} and crystal-field parameters in rare-earth titanate pyrochlores. *Phys. Rev. B* **2004**, *70*, 9. [CrossRef]

42. Raj, A.K.V.; Rao, P.P.; Sreena, T.S.; Sameera, S.; James, V.; Renju, U.A. Remarkable changes in the photoluminescent properties of $Y_2Ce_2O_7$: Eu^{3+} red phosphors through modification of the cerium oxidation states and oxygen vacancy ordering. *Phys. Chem. Chem. Phys.* **2014**, *16*, 23699–23710. [CrossRef] [PubMed]

43. Pavlov, R.S.; Marza, V.B.; Carda, J.B. Electronic absorption spectroscopy and colour of chromium-doped solids. *J. Mater. Chem.* **2002**, *12*, 2825–2832. [CrossRef]

44. Yamazaki, S.; Yamashita, T.; Matsui, T.; Nagasaki, T. Thermal expansion and solubility limits of plutonium-doped lanthanum zirconates. *J. Nucl. Mater.* **2001**, *294*, 183–187. [CrossRef]

45. Subramanian, M.A.; Aravamudan, G.; Subba Rao, G.V. Oxide pyrochlores—A review. *Prog. Solid State Chem.* **1983**, *15*, 55–143. [CrossRef]

46. Shannon, R.D. Revised effective ionic radii and systematic studies of interatomic distances in halides and chalcogenides. *Acta Crystallogr. Sect. A* **1976**, *32*, 751–767. [CrossRef]

47. Chartier, A.; Meis, C.; Weber, W.J.; Corrales, L.R. Theoretical study of disorder in Ti-substituted $La_2Zr_2O_7$. *Phys. Rev. B* **2002**, *65*, 11. [CrossRef]

48. Lian, J.; Wang, L.; Chen, J.; Sun, K.; Ewing, R.C.; Matt Farmer, J.; Boatner, L.A. The order–disorder transition in ion-irradiated pyrochlore. *Acta Mater.* **2003**, *51*, 1493–1502. [CrossRef]

49. Flores-Ruiz, H.M.; Naumis, G.G. Mean-square-displacement distribution in crystals and glasses: An analysis of the intrabasin dynamics. *Phys. Rev. E* **2012**, *85*, 041503. [CrossRef]

50. Shen, H.; Li, M.; Li, P.; Xiao, H.; Zhang, H.; Zu, X. Defect formation and its effect on the thermodynamic properties of Pu2Zr2O7 pyrochlore: A first-principles study. *J. Am. Ceram. Soc.* **2020**. [CrossRef]